Acta Pharmaceutica Sinica B 2025;15(9):4772−4788

Chinese Pharmaceutical Association
Institute of Materia Medica, Chinese Academy of Medical Sciences

Acta Pharmaceutica Sinica B

www.elsevier.com/locate/apsb
www.sciencedirect.com

ORIGINAL ARTICLE

Deubiquitinase OTUD6A alleviates acetaminophen-induced liver injury by targeting EZH2 to reduce cell death in hepatocytes

Yanni Zhao[a,b,c], Tianyang Jin[b], Tingxin Xu[b], Yi Fang[b], Qingsong Zheng[b], Wu Luo[b], Weiwei Zhu[a], Yue Chen[b], Jiong Wang[b], Yi Chen[b], Wei Zuo[d], Lijiang Huang[d], Guang Liang[a,b,e,*], Yi Wang[a,b,c,*]

[a]*Department of Cardiology, the First Affiliated Hospital of Wenzhou Medical University, Wenzhou Medical University, Wenzhou 325000, China*
[b]*Chemical Biology Research Center, School of Pharmaceutical Sciences, Wenzhou Medical University, Wenzhou 325035, China*
[c]*School of Pharmacy, Hangzhou Normal University, Hangzhou 311121, China*
[d]*Joint Research Center on Medicine, the Affiliated Xiangshan Hospital of Wenzhou Medical University, Ningbo 315700, China*
[e]*School of Pharmacy, Hangzhou Medical College, Hangzhou 311399, China*

Received 16 October 2024; received in revised form 30 January 2025; accepted 20 February 2025

KEY WORDS

Deubiquitinating enzyme;
OUT family;
OTUD6A;
Acetaminophen;
EZH2;
ER stress;
Cell death;
Liver injury

Abstract Acetaminophen (APAP) is the primary cause of drug-induced acute liver failure. Ovarian tumor deubiquitinase 6A (OTUD6A), a recently discovered deubiquitinase of the OTU family, has been primarily studied in tumor contexts. However, its role in APAP-induced liver injury (AILI) remains unclear. Therefore, this study aimed to investigate the involvement of OTUD6A in the pathogenesis of AILI. Our findings demonstrated a substantial upregulation of OTUD6A in both the liver tissue and isolated hepatocytes of mice following APAP stimulation. OTUD6A knockout exacerbated APAP-induced inflammation, hepatocyte necrosis, and liver injury, whereas OTUD6A overexpression alleviated these pathologies. Mechanistically, OTUD6A directly interacted with the enhancer of zeste homolog 2 (EZH2) and selectively removed K48-linked polyubiquitin chains from EZH2, enhancing its stability. This resulted in

*Corresponding authors.
E-mail addresses: yi.wang1122@hznu.edu.cn (Yi Wang), wzmcliangguang@163.com (Guang Liang).

Peer review under the responsibility of Chinese Pharmaceutical Association and Institute of Materia Medica, Chinese Academy of Medical Sciences.

https://doi.org/10.1016/j.apsb.2025.06.027

increased protein levels of EZH2 and H3K27me3, as well as reduced endoplasmic reticulum (ER) stress and cell death in hepatocytes. Collectively, our research uncovers a novel role for OTUD6A in mitigating APAP-induced liver injury by promoting EZH2 stabilization.

1. Introduction

Drug-induced liver injury (DILI) is a prevalent clinical problem worldwide, and the majority of cases of acute liver failure in Western countries are attributed to DILI[1,2]. Acetaminophen (*N*-acetyl-4-aminophenol, APAP) overdose is the leading cause of DILI[3]. APAP, commonly used as an antipyretic and analgesic, poses a significant risk of toxicity due to its wide usage in combination with other medications[4,5]. Excessive APAP consumption can lead to severe liver toxicity, making it the second leading cause of liver transplantation globally[6]. *N*-Acetylcysteine (NAC) is the primary therapy for APAP toxicity. However, oral administration of NAC can result in adverse effects such as nausea, vomiting, diarrhea, flatus, and gastroesophageal reflux[7]. Additionally, NAC has been associated with anaphylactoid reactions[8]. Therefore, investigating the regulatory mechanisms underlying APAP-induced acute liver injury and identifying novel therapeutic targets based on its pathogenesis shows significant clinical importance.

Ubiquitination has long been recognized as a crucial mechanism for determining the fate of proteins by tagging them for proteasomal degradation[9]. This process plays a crucial role in the development and progression of a range of diseases, including cancer, metabolic syndrome, neurodegenerative disorders, inflammatory and autoimmune diseases, infections, and muscular dystrophy[10]. Ubiquitination is a dynamic and reversible process, with E3 ubiquitin ligases and deubiquitinases (DUBs) playing prominent roles in regulating ubiquitin[11]. E3 ubiquitin ligase family NEDD4-1 protects against APAP-induced mitochondrial damage, necrosis, and liver injury through interacting with VDAC1 and mediates its K48-linked polyubiquitination and subsequent degradation[12]. Numerous DUBs, of which approximately 80 are predicted to be active in human cells, have been implicated in various human diseases, including neurodegeneration, inflammation, infection, and cancer[13]. Therefore, it is valuable to identify key modulators of ubiquitination that are involved in the pathological mechanisms of AILI.

Members of the OTU family, also known as OTU domain-containing DUBs, have emerged as key regulators of crucial signaling cascades, abnormal expression, and activation[14]. In the OTU family, OTUB1-mediated deubiquitination strengthens SLC7A11 stability, thereby activating system X_C^- to prevent carbon tetrachloride (CCl_4)-induced hepatocyte ferroptosis[15]. Another member, OTUD1, serves as a vital regulator of inflammation, oxidative stress responses, and reactive oxygen species (ROS)-associated cell death pathways[16]. OTUD4 negatively regulates TLR-mediated activation of NF-κB by targeting MyD88[17]. Ovarian tumor deubiquitinase 6A (OTUD6A) is a newly discovered deubiquitinase. Limited studies have investigated the role of OTUD6A in various cancers[18-20], and there have been no studies investigating the role of OTUD6A in AILI. In our present study, we demonstrate that OTUD6A plays a crucial role in suppressing APAP-induced endoplasmic reticulum (ER) stress, inflammation, cell death, and liver injury. Mechanistically, OTUD6A directly interacts with the enhancer of zeste homolog 2 (EZH2) and facilitates its K48-linked deubiquitination, leading to increased stability of EZH2. This stabilization of EZH2 by OTUD6A ultimately protects against APAP-induced endoplasmic reticulum (ER) stress, inflammation, cell death, and liver injury.

2. Materials and methods

2.1. Antibodies and reagents

4-Acetamidophenol (APAP, cat# A800441) was purchased from Shanghai Macklin Biochemical Technology (Shanghai, China). GSK126 (cat# 1346574-57-9) was from MCE (Shanghai, China). MG132 (cat# T2154) and Chloroquine (cat# T8689) were from TargetMol (Shanghai, China). Details regarding antibodies and other materials, along with their suppliers, can be found in the specific sections and Supporting Information Table S1.

2.2. Animal experiments

Approval for the care and experimental procedures involving mice was granted by the Wenzhou Medical University Animal Policy and Welfare Committee (Approval Document No. wydw2022-0202). The study utilized C57BL/6J (wild-type) mice, which were obtained from the university's Animal Center and weighed between 18 and 22 g. Additionally, *Otud6a*$^{-/-}$ mice on a C57BL/6J background were sourced from Professor Fuping You at the Peking University Health Science Center in Beijing, China[21]. All mice were maintained in a specific-pathogen-free facility, where environmental conditions were controlled at a temperature of 22 ± 2 °C and humidity levels of 50 ± 5%, following a 12 h light/dark cycle.

(1) To develop the APAP-induced liver injury model, male C57BL/6J or *Otud6a*$^{-/-}$ mice were fasted for 12 h, followed by the treatment of APAP (250 mg/kg, i.p.) for 6, 12, and 24 h.
(2) The hepatic *Otud6a* overexpression mouse model was established using AAV8. The AAV8 carrying *Otud6a* cDNA (NM_001163191) alongside a promoter (TBGp-MCS-3Flag-SV40 Poly A) was constructed by Genechem (Shanghai, China). AAV8 carrying *Otud6a* DNA (AAV8-OTUD6A, 1.5×10^{11} particles/mouse) was injected *via* the tail vein, while the control group received AAV8-empty vector (AAV8-Vector, 1.5×10^{11} particles/mouse). Two weeks post-injection of AAV8-OTUD6A or AAV8-Vector, liver injury was initiated with APAP (300 mg/kg) for 12 h.

(3) For liver-specific *Otud6a* knockdown, mice were injected with AAV8 vectors containing shRNA targeting the mouse *Otud6a* gene (AAV8-shOTUD6A) and a promoter (TBGp + chimeric intron-EGFP-MIR155(MCS)-WPRE-SV40 poly A), which was constructed by Genechem (Shanghai, China). Mice were injected in the lateral tail vein with 200 mL of virus containing 2.5×10^{11} AAV8 vector genomes. Two weeks post-injection of AAV8-shOTUD6A or AAV8-Vector, liver injury was initiated with APAP (300 mg/kg) for 12 h.
(4) EZH2 inhibitor, GSK126, was used to evaluate the protective role of OTUD6A in APAP-induced liver injury. Two weeks post-injection of AAV8-OTUD6A or AAV8-Vector, GSK126 (10 mg/kg) was administered to AAV8-Vector or AAV8-OTUD6A mice 12 h before APAP (300 mg/kg) administration and at the same time as APAP administration by intraperitoneal injection. Mice were sacrificed 12 h after APAP administration.

At different time intervals post-APAP administration, mice were anesthetized with isoflurane for subsequent analyses. Following the experiment, blood samples and liver tissues were harvested for further examination.

2.3. Cell culture

HEK-293T cells (cat# GNHu17) provided by the National Collection of Authenticated Cell Cultures (Shanghai, China) were cultured in DMEM (Gibco, Eggenstein, Germany) with 10% fetal bovine serum (FBS; Gibco). Primary hepatocytes were obtained from the liver of mice following the protocol described in our previously published paper[22].

2.4. Plasmid construction and transfection

OTUD6A-Flag and OTUD6A-C152A-Flag pcDNA3.1(+) plasmids were acquired from Tsingke Biotechnology in Beijing, China. In addition, expression pcDNA3.1(+) plasmids for Ub-Myc, Ub-K48-Myc, Ub-K63-Myc, Ub-K48R-Myc, EZH2-HA, EZH2-ΔSET-HA, EZH2-ΔCXC-HA, EZH2-K735R-HA, EZH2-K61R-HA, and EZH2-K569R-HA were obtained from KeLei Biological Technology located in Shanghai, China. All plasmid constructs were confirmed through DNA sequencing to ensure accuracy.

For transfection, the plasmids were temporarily transfected into HEK293T cells using Lipofectamine 3000 (cat# L3000015, Invitrogen, Waltham, MA) following the manufacturer's instructions.

2.5. Histological analysis

(1) Hematoxylin and eosin (H&E) staining: liver samples were formalin-fixed, paraffin-embedded, sectioned, and processed routinely for H&E staining.
(2) Immunohistochemical (IHC) staining: the expression profiles of OTUD6A, cleaved caspase 3, or CHOP in mouse liver samples were determined by incubating the liver sections with anti-OTUD6A, anti-cleaved caspase 3, or anti-CHOP primary antibodies, followed by specific secondary antibodies.
(3) TUNEL assay: frozen tissue sections with a thickness of 5 μm were obtained and first fixed in 4% paraformaldehyde for 10 min to facilitate permeabilization. Incubated with 0.1% Triton X-100. Afterward, the sections were treated with 5% bovine serum albumin for blocking for a duration of 30 min. 50 μL TUNEL was added and incubated in the dark at 37 °C for 60 min. Images were acquired using a fluorescent microscope at 200 × magnification (Nikon).

2.6. Immunofluorescence microscopy

Immunofluorescence staining was conducted on liver tissues using frozen samples embedded in OCT media, which were sectioned to a thickness of 5 μm. The sections were fixed in formalin for 10 min and subsequently blocked with 1% bovine serum albumin (BSA) for 1 h OTUD6A antibody was incubated overnight at 4 °C, followed by the application of fluorophore-conjugated secondary antibodies for 2 h at room temperature.

HEK-293T cells, which were transiently transfected with the relevant plasmids, were fixed in 4% paraformaldehyde for 10 min. The cells were then incubated overnight with anti-HA or anti-Flag antibodies. Following this incubation period, appropriate fluorophore-conjugated secondary antibodies were applied for 2 h at 37 °C. DAPI staining was used to visualize the nuclei. Images were acquired using a fluorescent microscope (Nikon).

2.7. Colorimetric assays

To assess liver injury induced by APAP, serum levels of alanine aminotransferase (ALT) and aspartate aminotransferase (AST) were measured. The enzymatic activities of ALT and AST were evaluated using commercial kits following the manufacturer's instructions. Liver glutathione (GSH) measurements were performed using commercially available kits and following the manufacturer's instructions.

2.8. RNA sequencing

Total RNA was isolated from the liver tissues of WT mice that were administered either PBS or APAP injections for 6 h, utilizing TRIzol reagent (cat# 15596018; Thermo Fisher). The quality of the extracted RNA was assessed through electrophoresis on a denaturing agarose gel. Subsequently, Poly(A) RNA was fragmented into smaller segments and reverse transcribed into complementary DNA (cDNA) with SuperScript II Reverse Transcriptase (cat# 1896649; Thermo Fisher). Following these pretreatments, the ligated products underwent amplification through PCR, creating a final cDNA library with an average fragment size of 300 ± 50 bp. For sequencing, 2 × 150 bp paired-end reads (PE150) were produced using an Illumina Novaseq 6000 (LC-BioTechnology Co., Ltd., Hangzhou, China). Differentially expressed genes (DEGs) were determined based on a fold change greater than 2 or less than 0.5, alongside a P value of less than 0.05. Gene-set enrichment analysis was conducted as outlined by Metascape (https://metascape.org/gp/index.html#/main/step1).

2.9. Mass spectrometry analysis

HEK-293T cells were transiently transfected with OTUD6A-Flag for 48 h, and the cells were harvested. Anti-Flag was added to HEK-293T lysates for the immunoprecipitation assay. Rabbit IgG was used as the negative control. Subsequently, LC−MS/MS analysis on a Thermo ScientificTM Q Exactive Plus mass spectrometer (Thermo Fisher Scientific) was performed by Jingjie PTM Biolabs (Hangzhou, China), and the resulting MS/MS data (Supporting Information Table S2) were analyzed *via* Proteome Discoverer v.1.3 (Thermo Fisher Scientific).

2.10. LC−MS/MS analysis

Blood samples were collected from the mice treated with APAP (300 mg/kg) for 1 h. After collection, the heparinized centrifugation tubes were spun at 3000 rpm for 10 min to separate the plasma. The serum samples were then stored at −20 °C in the freezer. Subsequently, 200 μL of the internal standard in acetonitrile was added to 40 μL of serum to extract the compound. Following 10 min of vortex mixing, the mixture was centrifuged at 8000 rpm for 10 min. The concentrations of samples were determined using the liquid chromatography and tandem mass spectrometry (LC−MS/MS) Triple 6500 plus system (SCIEX, CA, USA). The Agilent 1260 HPLC system coupled with an Agilent 6230 time of flight mass spectrometer (TOFMS) was employed for LC−TOF-MS analysis. The instrument was operated under negative ion mode using Jetstream electrospray ionization (ESI) as the ion source. A Phenomenex Clarity Oligo-MS column (2.1 mm × 150 mm, 2.6 μm) was used for separation by using TEA:HFIP:HO (0.4:30:1000, *v*/*v*/*v*) as mobile phase A and MeOH as mobile phase B. LC gradient is as follows: Initial conditions 95% A, 5% B, hold 1 min then a linear gradient starting at 1 min and ending at 16 min with 50% A and 50% B. The PK solver software was used to determine the pharmacokinetic parameters. The multiple reaction monitoring (MRM) conditions used for APAP were 152.1 → 110.0 with Collision Energy (CE) of 30 eV, Collision Accelerator Voltage (CAV) of 20 V. The MRM used for APAP-GLUT was 328.0 → 152.0 with CE of 30 V and CAV of 20 V. The MRM used for *N*-acetyl-*p*-benzoquinone imine (NAPQI) was 150.0 → 107.9 with CE of 30 V and CAV of 20 V. All analyses were obtained in the positive mode.

2.11. Immunoprecipitation and immunoblot analyses

For Western blot analysis, cell or tissue lysates were prepared using RIPA buffer (cat# P0013B; Beyotime Biological Technology), and protein concentrations were measured. Protein samples underwent SDS-PAGE and were transferred to PVDF membranes. The membranes were blocked for 1 h with a 5% skim milk buffer and then incubated overnight at 4 °C with primary antibodies. Afterward, they were exposed to horseradish peroxidase (HRP)-conjugated secondary antibodies for 1 h at room temperature. Immunoreactivity intensity was quantified using ImageJ software version 1.53i.

For immunoprecipitation (IP), total cellular protein was extracted using an immunoprecipitation RIPA buffer supplemented with a protease inhibitor. Protein lysates, ranging from 300 to 500 μg, were incubated overnight at 4 °C with a specific precipitating antibody. After incubation, the samples were combined with protein A + G agarose beads and gently mixed at room temperature for 4 h to promote immunoprecipitation. The resulting complexes of beads and proteins were then isolated by centrifugation and washed five times with PBS. Subsequently, these complexes were heated before being separated on an SDS-PAGE gel and analyzed through Western blotting using the relevant antibodies.

2.12. Real-time qPCR

Total RNA was isolated from cells and tissues using TRIzol Reagent (Thermo Fisher) according to the manufacturer's protocol. For the reverse transcription process, PrimeScript RT reagent (cat# RR047A, Takara Bioscience, Tokyo, Japan) was utilized. Real-time quantitative PCR was conducted using TB Green Premix Ex Taq II (cat# RR820A, Takara) on the CFX96 Touch Real-Time PCR Detection System (Bio-Rad). mRNA expression levels were normalized to the β-actin gene. The primer sequences employed in this study are listed in Supporting Information Table S3.

2.13. Statistical analysis

All data are reported as mean ± standard error of mean (SEM). Statistical analysis was performed with GraphPad Prism 8.0 software (San Diego, CA, USA). Student's *t*-test was employed for comparisons between two groups, whereas one-way ANOVA followed by Dunnett's *post hoc* test was used for analyzing multiple groups. For assessing mouse survival, Kaplan−Meier survival curves were generated, and the log-rank test was applied to evaluate significance. *P* value below 0.05 was considered statistically significant.

3. Results

3.1. OTUD6A expression is dramatically upregulated in hepatocytes of APAP-treated mice

Currently, there are few reports on the involvement of DUBs in AILI. In this study, we investigated the mRNA levels of all members of the OTU family of DUBs in the livers of both control and APAP-induced mice. Among these genes, the mRNA level of *Otud6a* was significantly increased in the livers of APAP-induced mice (Fig. 1A), indicating the potential association between OTUD6A and AILI. To further validate this finding, we performed Western blot analysis, immunofluorescence staining, and IHC staining. All results confirmed the upregulation of OTUD6A in the livers of APAP-induced mice (Fig. 1B−F). Next, we performed the immunofluorescence staining to determine the main cellular source of OTUD6A in the livers of APAP-treated mice. Immunofluorescence staining data showed that OTUD6A was mainly expressed in hepatocytes rather than macrophages in the liver (Fig. 1G and H). Subsequently, we isolated primary hepatocytes from WT mice and treated the cells with APAP. Our results showed a significant increase in OTUD6A protein levels at 1, 2, 4, and 8 h following APAP treatment (Fig. 1I and J). Furthermore, the mRNA level of *Otud6a* was significantly increased in APAP-challenged primary hepatocytes (Fig. 1K). Collectively, these findings confirm the upregulation of OTUD6A in both APAP-treated liver and hepatocytes.

3.2. OTUD6A deficiency exacerbates APAP-induced liver injury

We further investigated the role of OTUD6A in APAP-induced hepatotoxicity using *Otud6a* whole-body knockout ($Otud6a^{-/-}$) mice. The genotyping of $Otud6a^{-/-}$ mice is shown in Supporting Information Fig. S1A. As shown in Fig. 2A, the absence of OTUD6A intensified the APAP-induced liver injury, as evidenced by more extensive centrilobular necrosis, necrotic foci around the central vein, and hemorrhaging at different time points following APAP treatment (Fig. 2A and B). In addition, serum levels of ALT and AST were significantly higher in $Otud6a^{-/-}$ mice compared to the WT mice (Fig. 2C and D). Notably, $Otud6a^{-/-}$ mice exhibited a reduced survival rate compared to WT mice following exposure to a lethal dose (600 mg/kg) of APAP (Fig. 2E). Most researchers believe that when therapeutic concentrations of APAP enter the body, approximately 85% of APAP undergoes sulfation/glucuronidation to form complexes that are excreted *via* bile or urine, while approximately 15% undergoes conversion through the cytochrome P450 (CYP450) pathway, through which APAP is

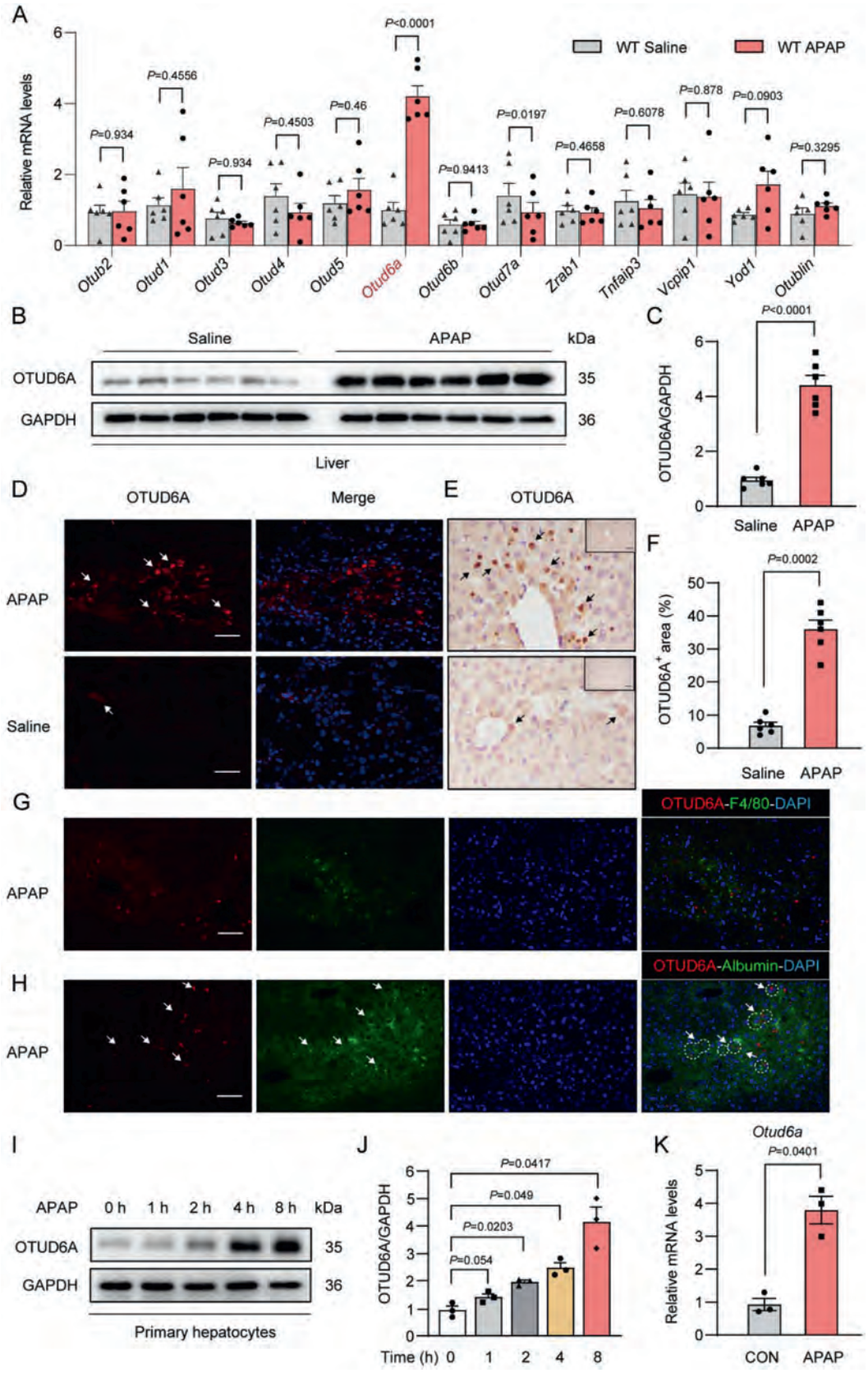

Figure 1 Hepatocyte OTUD6A expression is dramatically upregulated in the livers of APAP-treated mice. (A−H) Male C57BL/6J mice were fasted for 12 h and treated with APAP (300 mg/kg, i.p.) for 6 h. (A) The mRNA levels of members of the OTU family in the livers of saline- and APAP-treated mice were measured using RT-qPCR. The values were normalized to those of β-actin. (B) Representative images of Western blot analysis for OTUD6A expression in liver tissues of saline- and APAP-injected mice. GAPDH was used as the loading control. (C) The

converted to a toxic compound called NAPQI by an enzyme called P4502E1[23]. Excess APAP causes the accumulation of its toxic metabolite NAPQI, resulting in severe hepatotoxicity and hepatocellular necrosis[24]. Therefore, it is important to explore whether OTUD6A affects the metabolism of APAP in mice. We performed LC−MS/MS to measure plasma APAP and APAP metabolites after APAP administration in WT and *Otud6a*$^{-/-}$ mice. Our results indicate that WT mice and *Otud6a*$^{-/-}$ mice have similar APAP metabolites after APAP administration for 1 h (Fig. S1B−S1D). These results demonstrate that OTUD6A has no significant effect on the metabolic activation of APAP.

To clarify the mechanisms through which OTUD6A protects against APAP-induced liver injury, we performed RNA sequencing on liver tissues from the APAP-treated cohorts. As shown in Fig. S1E, we identified 3327 differentially expressed genes, comprising 1134 genes that were upregulated and 2193 genes that were downregulated in the *Otud6a*$^{-/-}$APAP group compared to the WT-APAP group. Meta Scape analysis revealed significant alterations in processes related to programmed cell death and inflammatory responses in the *Otud6a*$^{-/-}$APAP group relative to the WT-APAP group (Fig. S1F). We next assessed how OTUD6A regulates inflammatory and cell apoptosis in APAP-induced liver. Our results showed the mRNA levels of inflammatory cytokines were markedly higher in the *Otud6a*$^{-/-}$APAP group when compared to those of the WT-APAP group (Fig. 2F and G). In addition, TUNEL staining confirmed that *Otud6a*$^{-/-}$ enhanced DNA double-strand breaks induced by APAP in the liver (Fig. 2H and I). Subsequently, we constructed AAV8-shOTUD6A with the hepatocyte-specific promoter to specifically investigate the role of hepatic OTUD6A in APAP-induced liver injury. AAV8-shOTUD6A was administered to C57BL/6 mice *via* tail vein injection. Two weeks later, we performed WB and RT-qPCR analyses to ascertain the OTUD6A knockout efficiency. The results indicated that OTUD6A was significantly reduced at both the protein (Supporting Information Fig. S2A and S2B) and mRNA levels in the AAV8-shOTUD6A group compared to those in the AAV8-Vector group (Fig. S2C). Mice were then treated with APAP *via* intraperitoneal injection (Supporting Information Fig. S3A). Histological analysis revealed that AAV8-shOTUD6A administration increased signs of liver injury (Fig. S3B and S3C). In addition, AAV8-shOTUD6A administration aggravated APAP-induced increases of ALT and AST (Fig. S3D and S3E), indicating impaired liver function. Hepatic GSH levels were significantly lower in AAV8-shOTUD6A than in AAV8-Vector mice (Fig. S3F). TUNEL staining demonstrated that administration of AAV8-shOTUD6A significantly enhanced APAP-induced hepatic DNA damage (Fig. S3G and S3H). Collectively, these results demonstrate that OTUD6A hepatocyte-specific deficiency exacerbates APAP-induced liver injury and necrosis, suggesting a critical protective function of OTUD6A in preserving liver integrity under conditions of hepatotoxic stress.

3.3. Hepatic overexpression of OTUD6A alleviates APAP-induced liver injury

To further validate the role of hepatocyte OTUD6A in liver injury induced by APAP, we overexpressed OTUD6A in the liver using AAV8 (AAV8-OTUD6A) to assess the response to APAP treatment (Fig. 3A). Western blot analysis confirmed successful overexpression of OTUD6A in the livers of mice injected with AAV8-OTUD6A (Supporting Information Fig. S4A). One hour after APAP dosing, AAV8-Vector and AAV8-OTUD6A mice had equivalent serum concentrations of APAP and APAP metabolites, including NAPQI and APAP glucuronide (Fig. S4B−S4D). Mice injected with AAV8-OTUD6A exhibited less liver injury and necrosis in response to APAP administration compared to those given the AAV8-vector, as evidenced by a reduction in necrotic area (Fig. 3B and C) and lower serum levels of ALT (Fig. 3D) and AST (Fig. 3E). Additionally, overexpression of OTUD6A significantly improved the survival rate of mice following a lethal dose (600 mg/kg) of APAP (Fig. 3F). RT-qPCR analysis demonstrated a marked reduction in the expression of inflammatory genes in the AAV8-OTUD6A group compared to the AAV8-vector group (Fig. 3G and H). In addition, TUNEL staining revealed that hepatocyte DNA damage induced by APAP was significantly lower in mice overexpressing OTUD6A compared to those injected with the AAV8-vector (Fig. 3I and J). Overall, these findings indicate that OTUD6A exerts a protective effect against APAP-induced hepatotoxicity, underscoring its potential as a therapeutic target for interventions aimed at liver injury.

3.4. OTUD6A directly interacts with EZH2

Next, we sought to identify the potential binding target of OTUD6A. We overexpressed Flag-OTUD6A in HEK293T cells and immunoprecipitated Flag-tagged OTUD6A, followed by mass spectrometry analysis to identify potential OTUD6A binding candidates (Fig. 4A). Among the potential binding proteins, we focused on EZH2. EZH2 serves as a key catalytic component of the polycomb repressive complex 2 (PRC2), playing a crucial role in gene silencing[25]. It achieves this by catalyzing the trimethylation of lysine 27 on histone H3 (H3K27me3) in the promoter regions of genes[26]. EZH2 has been identified to play essential roles in liver injury[27,28]. Representative MS spectra of EZH2 are shown in Fig. 4B. The interaction between EZH2 and OTUD6A was confirmed through co-immunoprecipitation experiments in HEK293T cells (Fig. 4C−E), as well as immunofluorescence staining of OTUD6A-Flag and EZH2-HA co-transfected cells

densitometric quantification data for Fig. 1B were determined by Image J. (D) Immunofluorescence staining for OTUD6A (red) in the liver tissues from saline- and APAP-treated mice. Sections were counterstained with DAPI (blue); scale bar = 50 μm. (E) Representative immunohistochemical staining images of liver tissues obtained from mice treated with saline or APAP. Immunoreactivity was detected using DAB staining (brown). Sections were counterstained with hematoxylin (blue); scale bar = 50 μm. (F) Quantification of OTUD6A staining positive area in Fig. 1E. (G) Representative staining images showing immunoreactivity to OTUD6A (red) and macrophage marker F4/80 (green). Tissues were counterstained with DAPI (blue); scale bars = 25 μm. (H) Representative immunofluorescence staining images of normal mouse liver tissues showing immunoreactivity to OTUD6A (red) and hepatocyte marker albumin (green). Tissues were counterstained with DAPI (blue). Arrows indicating co-localization; scale bars = 25 μm. (I) Representative Western blotting images of OTUD6A expression in primary hepatocytes treated with 15 mmol/L APAP for different times (1, 2, 4, or 8 h). GAPDH was used as the loading control. (J) The densitometric quantification data for Fig. 1I was shown. (K) The mRNA levels of *Otud6a* in response to 6 h-stimulation of APAP (15 mmol/L) in primary hepatocytes. The values were normalized to *Actb*. Statistical data are presented as mean ± SEM; $n = 6$ for *in vivo* experiments and $n = 3$ for *in vitro* experiments.

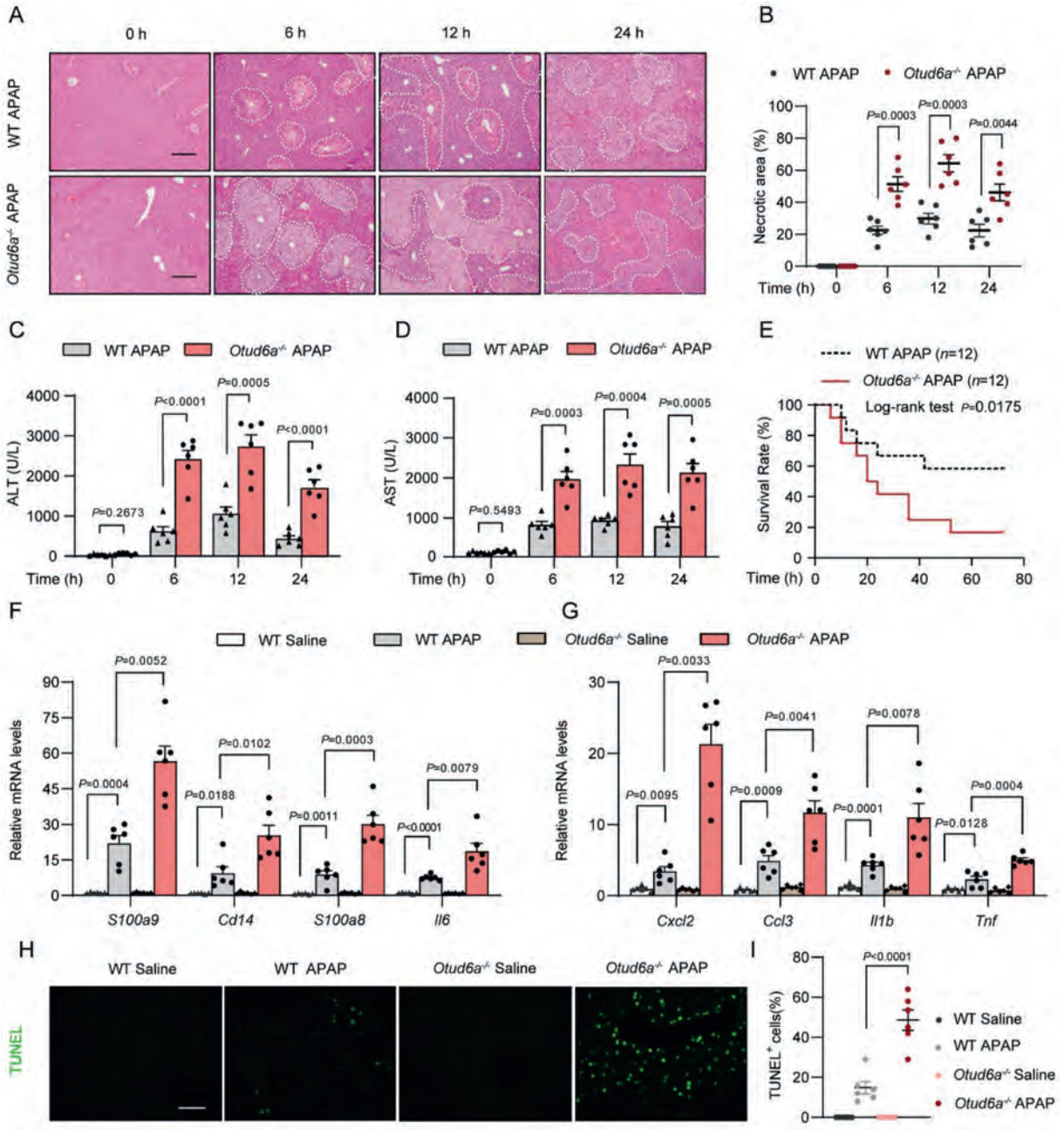

Figure 2 Deficiency of OTUD6A exacerbates APAP-induced liver injury *in vivo*. (A−D) WT and *Otud6a*$^{-/-}$ mice were treated with APAP (250 mg/kg, i.p., $n = 6$). Liver tissues and serum samples were harvested at 0, 6, 12, and 24 h post-APAP treatment. (A) Representative images of H&E staining for liver tissues at different time points after APAP treatment (scale bar = 100 μm) and necrotic areas were quantified (B). Serum levels of ALT (C) and AST (D) were assayed using commercial kits ($n = 6$). (E) WT and *Otud6a*$^{-/-}$ mice were treated with a lethal dose of APAP (600 mg/kg, i.p., $n = 12$). Survival rates were recorded. (F−I) WT and *Otud6a*$^{-/-}$ mice were treated as mentioned in Fig. 2A. Liver tissue samples were harvested at 12 h post-APAP treatment. (F, G) mRNA levels of inflammatory factors in the liver tissues of mice were measured using RT-qPCR. Transcripts were normalized to *Actb* ($n = 6$). (H, I) Representative images of TUNEL-stained liver sections (scale bar = 50 μm) and the quantification for the TUNEL-staining are shown. Statistical data are presented as mean ± SEM, $n = 6$.

(Fig. 4F). EZH2 consists of various distinct regions, including the EED-interaction domain (EID), Domain I, Domain II, a cysteine-rich region (CXC domain), and the C-terminal SET domain, which is linked to the functions of suppressor of variegation 39, enhancer of zeste, and trithorax[29]. To better understand the interaction between OTUD6A and EZH2, we designed a series of truncated EZH2 proteins. This approach aimed to identify the specific domains or regions that mediate the interaction (Fig. 4G). Interestingly, OTUD6A could bind to EZH2 without the CXC or the SET domain (Fig. 4H). Additionally, our analysis revealed that exogenously expressed OTUD6A elevated the protein levels of EZH2 in HEK293T cells, while the catalytic-dead mutant

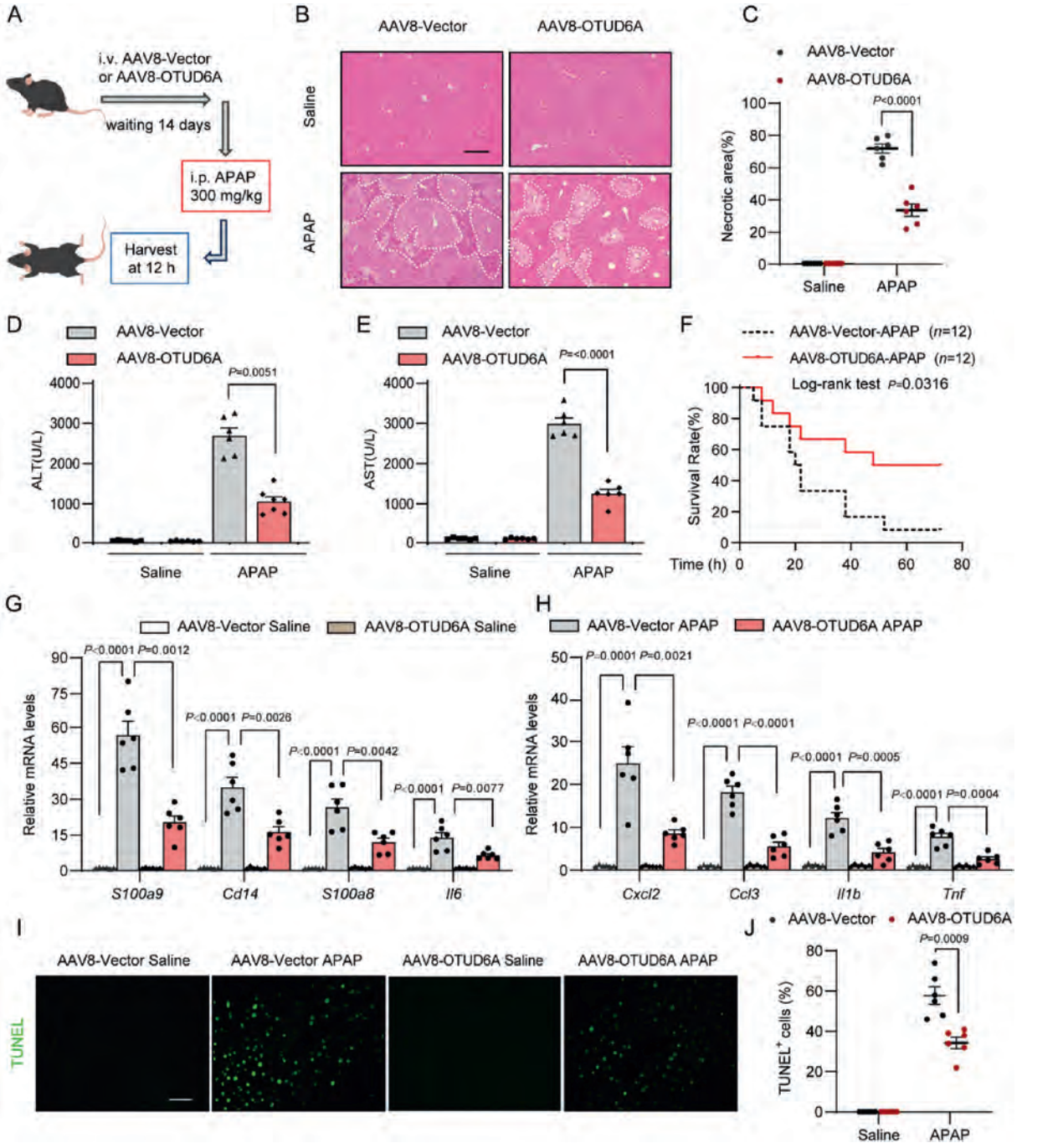

Figure 3 OTUD6A overexpression significantly prevents APAP-induced liver injury and necrosis. (A) Schematic strategy for generating OTUD6A overexpression mice (AAV8-OTUD6A) and the experimental timeline of the APAP-induced liver injury mouse model. (B, C) Representative images of H&E-stained liver sections (scale bar = 100 μm) and the quantified necrotic areas ($n = 6$) were shown. (D, E) Serum levels of ALT and AST were assayed using commercial kits ($n = 6$). (F) Survival rates of AAV-Vector and AAV-OTUD6A mice following treatment with a lethal dose of APAP (600 mg/kg, i.p., $n = 12$) are shown. (G−K) AAV-vector and AAV-OTUD6A mice were treated as mentioned in panel (A). Liver tissue samples were harvested at 12 h post-APAP treatment. (G, H) mRNA levels of inflammatory genes in the liver tissues of mice. Transcripts were normalized to *Actb* ($n = 6$). (I, J) Representative images of TUNEL-stained liver sections (scale bar = 50 μm) and the quantification for the TUNEL-staining were shown ($n = 6$). Statistical data are presented as mean ± SEM.

$OTUD6A^{C152A}$ did not produce the same effect (Fig. 4I and J). Finally, to demonstrate whether the interaction between endogenous OTUD6A and EZH2 occurs in primary mouse hepatocytes, we performed immunoprecipitation of either endogenous OTUD6A or EZH2 from these cells (Fig. 4K). The results in Fig. 4K indicate that the interaction between OTUD6A and EZH2 was enhanced following the APAP challenge. These data confirm that OTUD6A interacts with EZH2.

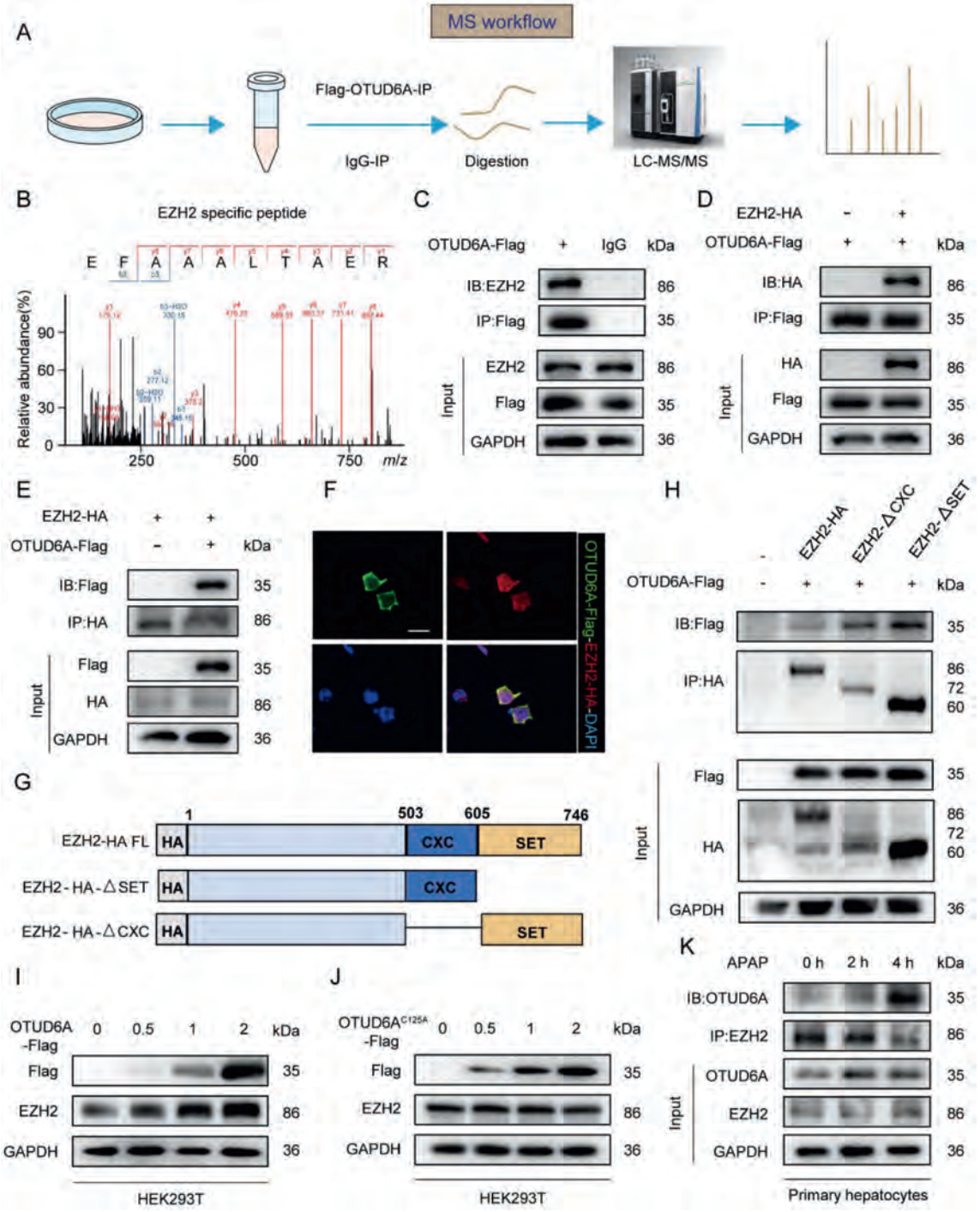

Figure 4 OTUD6A directly interacts with EZH2. (A) Schematic illustration of the quantitative proteomic screening for identification of OTUD6A-binding proteins. (B) MS/MS spectrum data showing the peptide sequences of the OTUD6A-binding substrate. *m/z* = mass/charge ratio. (C−E) HEK-293T cells were transfected with Flag-tagged OTUD6A alone or co-transfected with HA-tagged EZH2 plasmids. Lysates from cells were immunoprecipitated with anti-Flag or anti-HA antibodies. EZH2 and OTUD6A levels were detected with specific antibodies using immunoblotting assays. (F) Colocalization between OTUD6A and EZH2 was examined by fluorescence microscopy in HEK293T cells co-transfected with Flag-tagged OTUD6A and HA-tagged EZH2 plasmids. (G) Schematic diagram of EZH2 and its truncated mutants. (H) Plasmids of HA-tagged EZH2 or its truncated mutants and plasmids of Flag-tagged OTUD6A were transfected into HEK293T cells. Lysates from cells were immunoprecipitated with anti-HA antibodies. OTUD6A levels were detected using immunoblotting assays. (I, J) HEK-293T cells were transfected with different doses (0, 0.5, 1, 2 μg) of Flag-tagged OTUD6A (I) or Flag-tagged OTUD6A^{C125A} (J) plasmids. EZH2 levels were detected using immunoblotting assays. GAPDH was used as the loading control. (K) The interaction of endogenous OTUD6A and EZH2 in APAP-stimulated primary hepatocytes was measured using co-IP assays. Representative images of all immunoblot data are shown, and similar results were obtained from three independent experiments ($n = 3$).

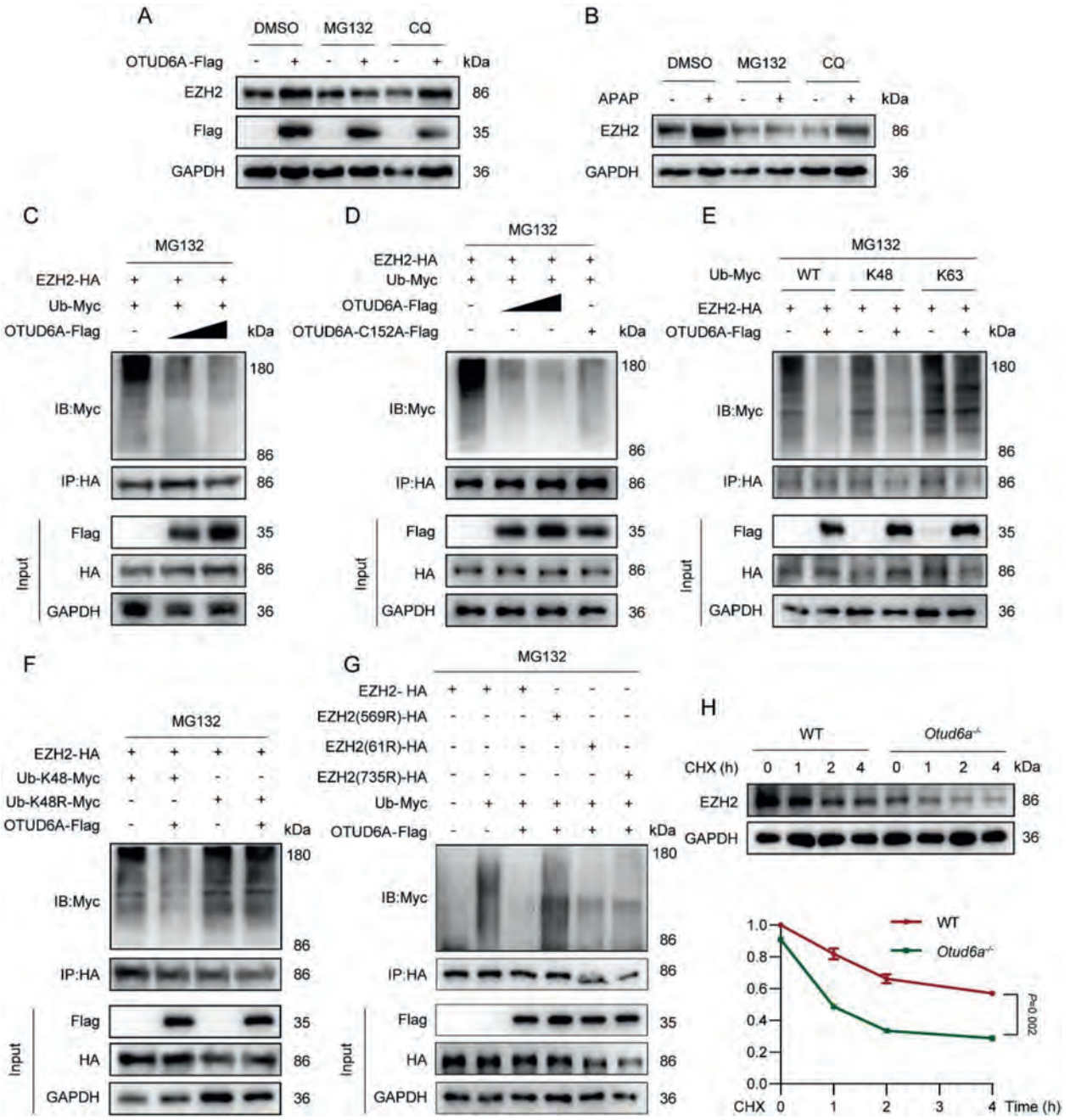

Figure 5 EZH2 is the potential substrate of OTUD6A in hepatocytes. (A) Primary hepatocytes were transfected with Flag-Vector or Flag-OTUD6A plasmids, followed by treatment with MG132 (10 μmol/L) or CQ (50 μmol/L). Protein levels of EZH2 were measured using Western blotting assays. (B) Primary hepatocytes were treated with APAP (10 mmol/L) for 12 h. Cells were treated with MG132 (10 mmol/L), CQ (50 mmol/L), or vehicle control (DMSO, 1‰) 6 h post-ATAP stimulation. Cells were harvested 12 h post-APAP treatment. The protein levels of EZH2 were measured using Western blotting assays. (C) HEK-293T cells were co-transfected with plasmids of Ub-Myc, EZH2-HA, and increasing concentrations of OTUD6A-Flag, followed by IP with anti-HA magnetic beads. Cells were treated with MG132 (10 μmol/L) for 6 h before harvesting. The ubiquitination of EZH2 was measured by immunoblot analysis. (D) Immunoblot analysis of the ubiquitination of EZH2 in HEK293T cells co-transfected with Ub-Myc, EZH2-HA, and increasing concentrations of OTUD6A-Flag or OTUD6A-C152A-Flag vectors. (E) Immunoblot analysis of the ubiquitination of EZH2 in HEK293T cells co-transfected with EZH2-HA, OTUD6A-Flag, and various types of Ub-Myc, including WT, K48-, and K63-linked ubiquitin chains for 24 h. (F) Immunoblot analysis of the ubiquitination of EZH2 in HEK293T cells co-transfected with EZH2-HA, OTUD6A-Flag, Ub-K48-Myc, or Ub-K48R-Myc. (G) Immunoblot analysis of the ubiquitination of EZH2 in HEK293T cells co-transfected with OTUD6A-Flag, Ub-Myc, and EZH2-HA, or mutant EZH2-HA, including EZH2 (569R)-HA, EZH2 (61R)-HA, and EZH2 (735R)-HA. (H) Primary hepatocytes derived from WT or *Otud6a*$^{-/-}$ mice were treated with cycloheximide (CHX, 100 μg/mL) at the indicated time points. Cell lysates were then collected for immunoblotting. The representative image of EZH2 expression (upper panel) and the quantification of the protein levels of EZH2 (lower panel) are shown. Statistical data are presented as mean ± SEM; $n = 3$.

3.5. OTUD6A regulates the stability of EZH2 through deubiquitination

Previous results have indicated that OTUD6A overexpression significantly increased the protein abundance of EZH2 (Fig. 4I). To investigate the underlying mechanisms, we treated cells with proteasome and lysosome inhibitors to evaluate the role of these cellular pathways in EZH2 regulation. Our findings indicated that the proteasome inhibitor MG132 effectively prevented the rise in EZH2 protein levels, whereas the lysosome inhibitor chloroquine (CQ) did not have the same effect (Fig. 5A and B). This suggests that OTUD6A plays a role in regulating the proteasomal degradation of EZH2. Next, to investigate whether OTUD6A promotes the deubiquitination of EZH2, we transfected HEK-293T cells with plasmids expressing Myc-tagged ubiquitin, HA-tagged EZH2, and Flag-tagged OTUD6A. We administered MG132 to the cells to inhibit the proteasomal degradation of EZH2 and discovered that OTUD6A decreased the ubiquitination levels of EZH2 (Fig. 5C). In contrast, the OTUD6A^{C152A} mutant did not exhibit this activity (Fig. 5D). Additionally, to determine the type of ubiquitin chain affected by OTUD6A on EZH2, we co-transfected EZH2, OTUD6A, and mutated ubiquitin plasmids that retain only K48 or K63 active sites in HEK-293T cells, followed by the MG132 treatment. Fig. 5E shows that OTUD6A primarily removed the K48-linked ubiquitin chains from EZH2. Consistently, the K48R mutation counteracted the deubiquitination activity of OTUD6A on EZH2 (Fig. 5F), suggesting that OTUD6A primarily facilitates K48-linked deubiquitination of EZH2. We explored ubiquitinated lysine residues in the EZH2 protein using the prediction online tool (http://gpsuber.biocuckoo.cn/online.php). The prediction result showed that EZH2-K61, EZH2-K569, and EZH2-K735 are the top three sites. Subsequently, we mutated active sites on EZH2 (K61R, K569R, and K735R). We found that OTUD6A could not deubiquitinate EZH2 after mutating K569 but could still be deubiquitinated by OTUD6A after mutating K61 and K735 (Fig. 5G). Finally, we conducted a cycloheximide (CHX) chase assay, which revealed that the absence of OTUD6A significantly reduced the half-life of the endogenous EZH2 protein in primary mouse hepatocytes (Fig. 5H). In summary, these results show that OTUD6A removes ubiquitin molecules from EZH2, thereby preventing its degradation.

3.6. OTUD6A mediates APAP-induced ER stress and cell death via EZH2 in primary mouse hepatocytes

EZH2 is widely recognized for its role as a histone methyltransferase, where it inhibits gene expression through the trimethylation of H3K27[30]. Compared to WT hepatocytes, the levels of EZH2 and H3K27me3 were markedly lower in *Otud6a*$^{-/-}$ hepatocytes (Fig. 6A−C). It has been reported that preserving H3K27 methylation could ameliorate the ER stress[31]. Importantly, in APAP-treated hepatocytes, ER stress can be initiated and trigger cellular necrosis if excessively severe or prolonged[32,33]. Thus, we examined mRNA levels of ER stress cytokines in APAP-treated primary hepatocytes. The results indicate that OTUD6A deficiency led to elevated levels of cytokines associated with ER stress (Fig. 6D). Similarly, OTUD6A deficiency resulted in higher levels of ER stress protein compared with those in WT hepatocytes (Fig. 6E, Supporting Information Fig. S5A and S5B). In addition, mRNA levels of inflammatory cytokines were significantly higher in *Otud6a*$^{-/-}$ hepatocytes than in WT hepatocytes (Fig. 6F and G), suggesting that OTUD6A in primary mouse hepatocytes mediates APAP-induced ER stress and inflammation.

To further confirm the function of OTUD6A *in vitro*, primary hepatocytes isolated from WT mice were transfected with either the OTUD6A plasmid or control vector before being subjected to APAP treatment. Consistent with the results *in vivo*, overexpression of OTUD6A in primary hepatocytes also alleviated APAP-induced ER stress (Fig. 7A and B, Fig. S5C and S5D). Cellular inflammation was also significantly reduced after OTUD6A overexpression (Fig. 7C−E). Subsequently, to verify that EZH2 plays an important role in OTUD6A-regulated ER stress and cell apoptosis induced by APAP, we used an EZH2 inhibitor, GSK126, to examine the changes of related proteins after OTUD6A overexpression. As shown in Fig. 7F−J, GSK126 treatment significantly reversed the anti-ER stress and anti-inflammatory effects of OTUD6A at both the mRNA (Fig. 7F−I) and protein levels (Fig. 7J, Fig. S5E−S5G) in APAP-treated primary mouse hepatocytes. Taken together, our data show that OTUD6A mediates ER stress and cell death in APAP-challenged primary mouse hepatocytes by targeting EZH2.

3.7. OTUD6A mediates APAP-induced ER stress via EZH2 in the liver

Finally, we confirmed the regulatory effects of OTUD6A on APAP-induced acute liver injury *in vivo*. Our results show that EZH2 and H3K27me3 levels were decreased in APAP-treated *Otud6a*$^{-/-}$ mice compared to the WT mice (Fig. 8A and B). Consistent with these findings, OTUD6A deficiency exacerbated the APAP-induced ER stress, as evidenced by increased mRNA and protein levels of ER stress-related factors in the *Otud6a*$^{-/-}$ mice (Supporting Information Fig. S6A−S6E). IHC staining results confirm the increased CHOP expression in the livers of APAP-treated *Otud6a*$^{-/-}$ mice (Fig. S6F). The overexpression of OTUD6A in the liver significantly reduced the APAP-induced ER stress-related proteins at mRNA and protein levels (Supporting Information Fig. S7A−S7E). Finally, we explored whether the pharmacologic inhibition of EZH2 could reverse the protective effect of OTUD6A in APAP-induced liver injury. We employed the EZH2 inhibitor, GSK126, to validate the role of the OTUD6A-EZH2 axis (Fig. 8C). With the treatment of GSK126, OTUD6A overexpression failed to reverse APAP-induced liver injury, as evidenced by higher serum levels of AST (Fig. 8D) and ALT (Fig. 8E), and increased necrotic area in the liver (Fig. 8F and G). Furthermore, TUNEL staining demonstrated that GSK126 administration significantly increased APAP-induced hepatic cell DNA fragmentation compared to the AAV2/8-OTUD6A group (Fig. 8H and I). Collectively, these results demonstrate that pharmacologic inhibition of EZH2 reverses the protective effect of OTUD6A in APAP-induced liver injury. Based on the *in vivo* and *in vitro* results, we conclude that OTUD6A overexpression ameliorates APAP-induced ER stress in the liver by maintaining the stability and activity of EZH2.

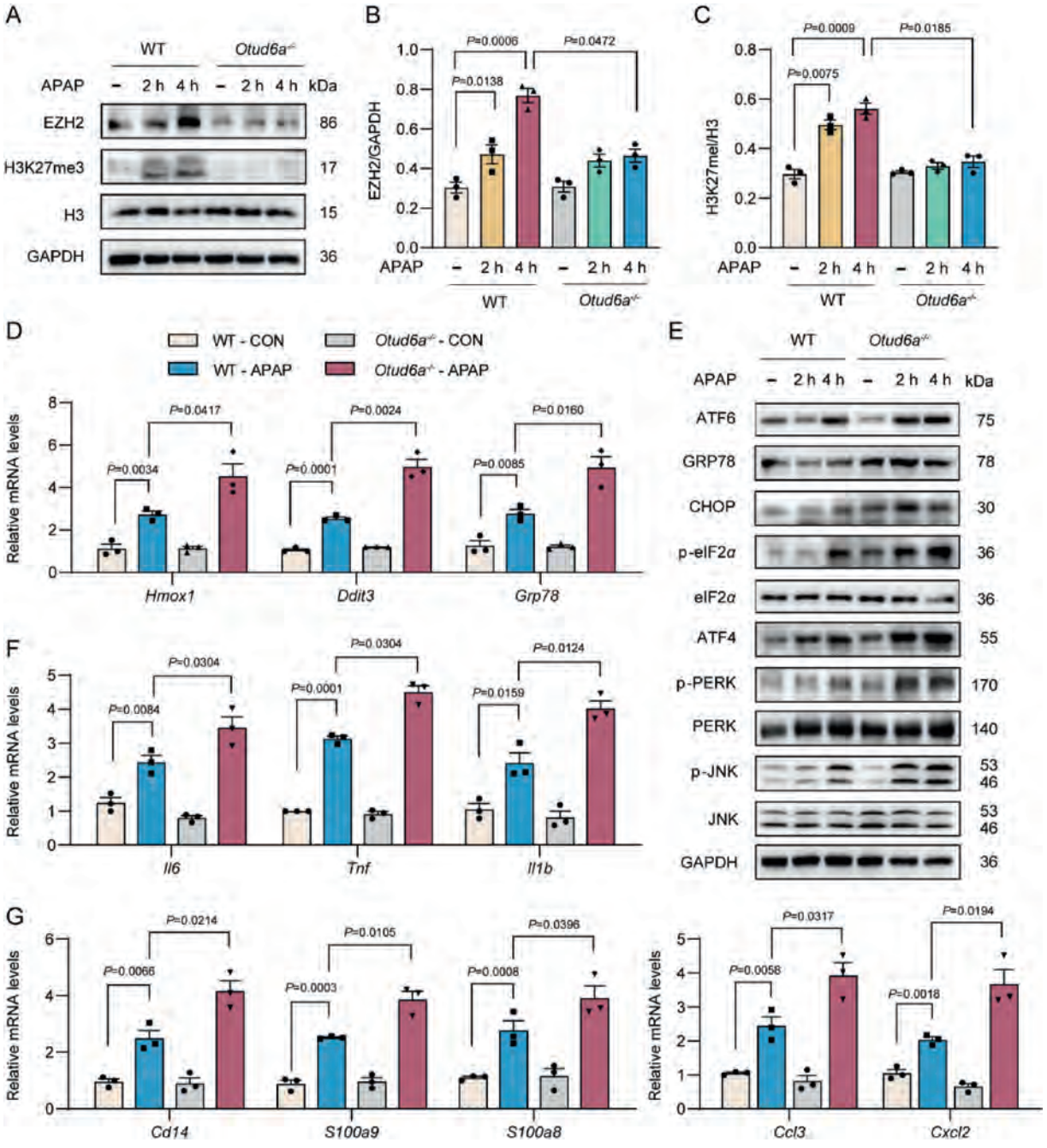

Figure 6 OTUD6A deubiquitinates EZH2 and protects hepatocytes from APAP-induced cell death *via* alleviating ER stress. Primary hepatocytes isolated from WT and *Otud6a*$^{-/-}$ mice were treated with 15 mmol/L APAP for various time points. (A) The protein levels of EZH2, H3K27me3, and H3 in the primary hepatocytes were determined by Western blotting assays. Representative immunoblots are shown. GAPDH was used as the loading control. (B, C) The densitometric quantification data for Fig. 6A are shown. (D) mRNA levels of endoplasmic reticulum (ER) factors (*Hmox1*, *Ddit3*, and *Grp78*) in cell lysates. Transcripts were normalized to *Actb*. (E) Measurement of ER proteins (ATF6, GRP78, CHOP, *p*-eIF2α, eIF2α, ATF4, p-PERK, PERK, *p*-JNK, and JNK) in cell lysates. Representative immunoblots are shown. GAPDH was used as the loading control. (F, G) mRNA levels of inflammatory genes in cell lysates. Transcripts were normalized to *Actb*. All the statistical data are presented as mean ± SEM; $n = 3$.

4. Discussion

In this study, we investigated the function of OTUD6A in acute liver injury induced by APAP, using both *in vivo* and *in vitro* approaches. Our findings indicate that the knockout of OTUD6A exacerbated APAP-induced ER stress and apoptosis, which can be attributed to the decreased stability of EZH2. Additionally, we uncovered the mechanism by which OTUD6A activates EZH2: 1) OTUD6A directly interacts with EZH2; 2) OTUD6A cleaves K48-linked polyubiquitin chains on EZH2 at lysine 569, thereby preventing its proteasomal degradation and enhancing the stability and levels of EZH2; 3) OTUD6A

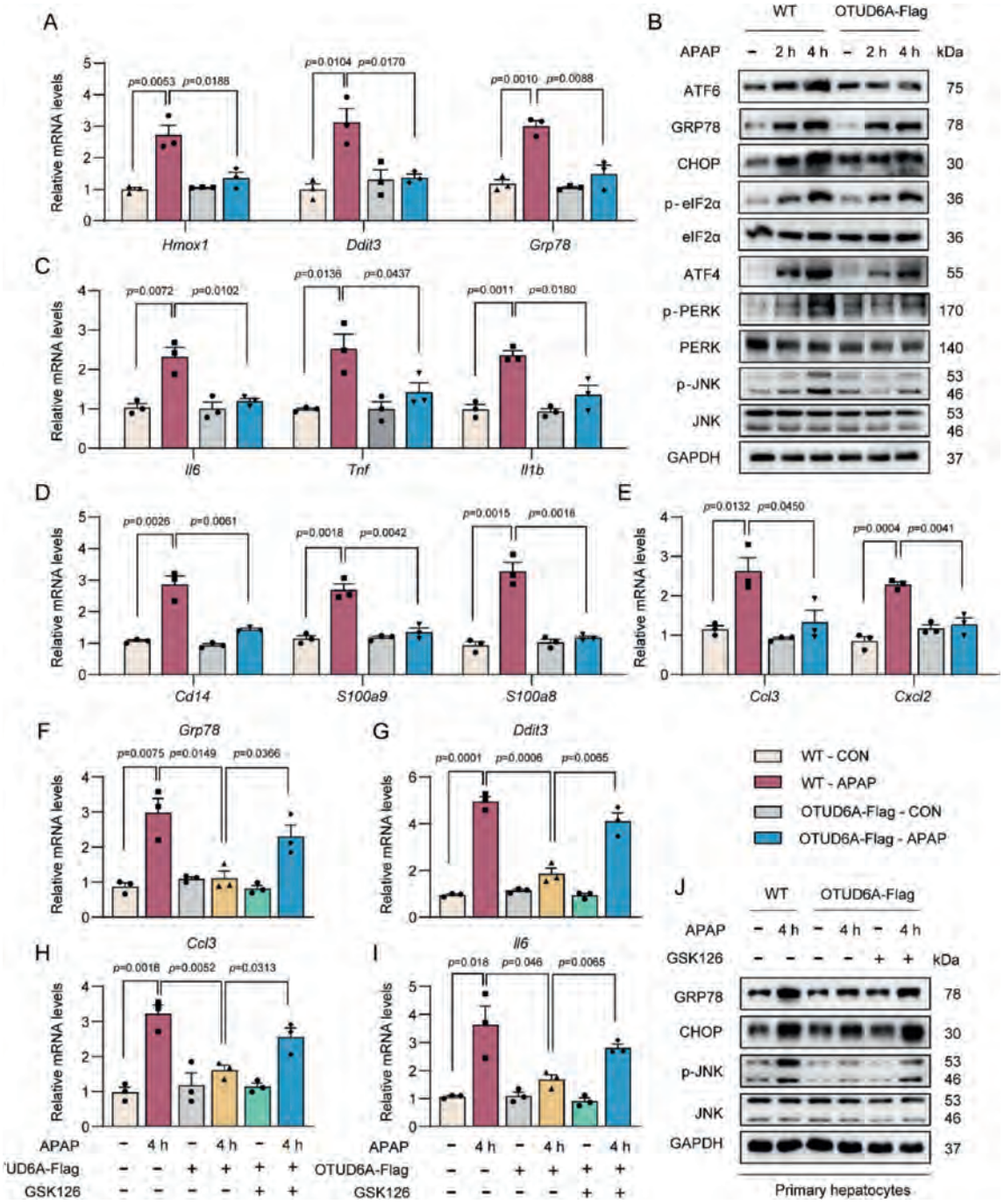

Figure 7 Pharmacologic inhibition of EZH2 reverses the protective effect of OTUD6A in APAP-challenged hepatocytes. (A−E) Primary hepatocytes from WT mice were transfected with the OTUD6A plasmid to overexpress OTUD6A, followed by a challenge of 15 mmol/L APAP for various time points. (A) mRNA levels of ER factors in cell lysates. Transcripts were normalized to *Actb*. (B) Measurement of ER proteins in cell lysates. Representative immunoblots are shown. GAPDH was used as the loading control. (C−E) mRNA levels of inflammatory genes in cell lysates. Transcripts were normalized to *Actb*. (F−J) Primary hepatocytes were transfected with OTUD6A plasmid and treated with the EZH2 inhibitor, GSK126 (2 μmol/L), or vehicle control (DMSO) for 72 h, followed by an APAP challenge (15 mmol/L) for 4 h. (F−I) mRNA levels of ER and inflammatory genes in cell lysates. Transcripts were normalized to *Actb*. (J) Measurement of ER and apoptosis-related proteins (GRP78, CHOP, *p*-JNK, and JNK) in cell lysates. Representative immunoblots are shown. GAPDH was used as the loading control. Statistical data are presented as mean ± SEM; $n = 3$.

elevation of EZH2 and H3K27me3 protein levels in primary hepatocytes treated with APAP contributed to decreased ER stress and reduced hepatocyte death. A schematic overview of these key findings is illustrated in the graphical abstract. In conclusion, our data suggest that targeting the OTUD6A−EZH2 axis may represent a viable therapeutic approach for DILI.

DUBs play essential roles in maintaining protein homeostasis and quality control by precisely regulating the equilibrium between ubiquitination and deubiquitination in physiological

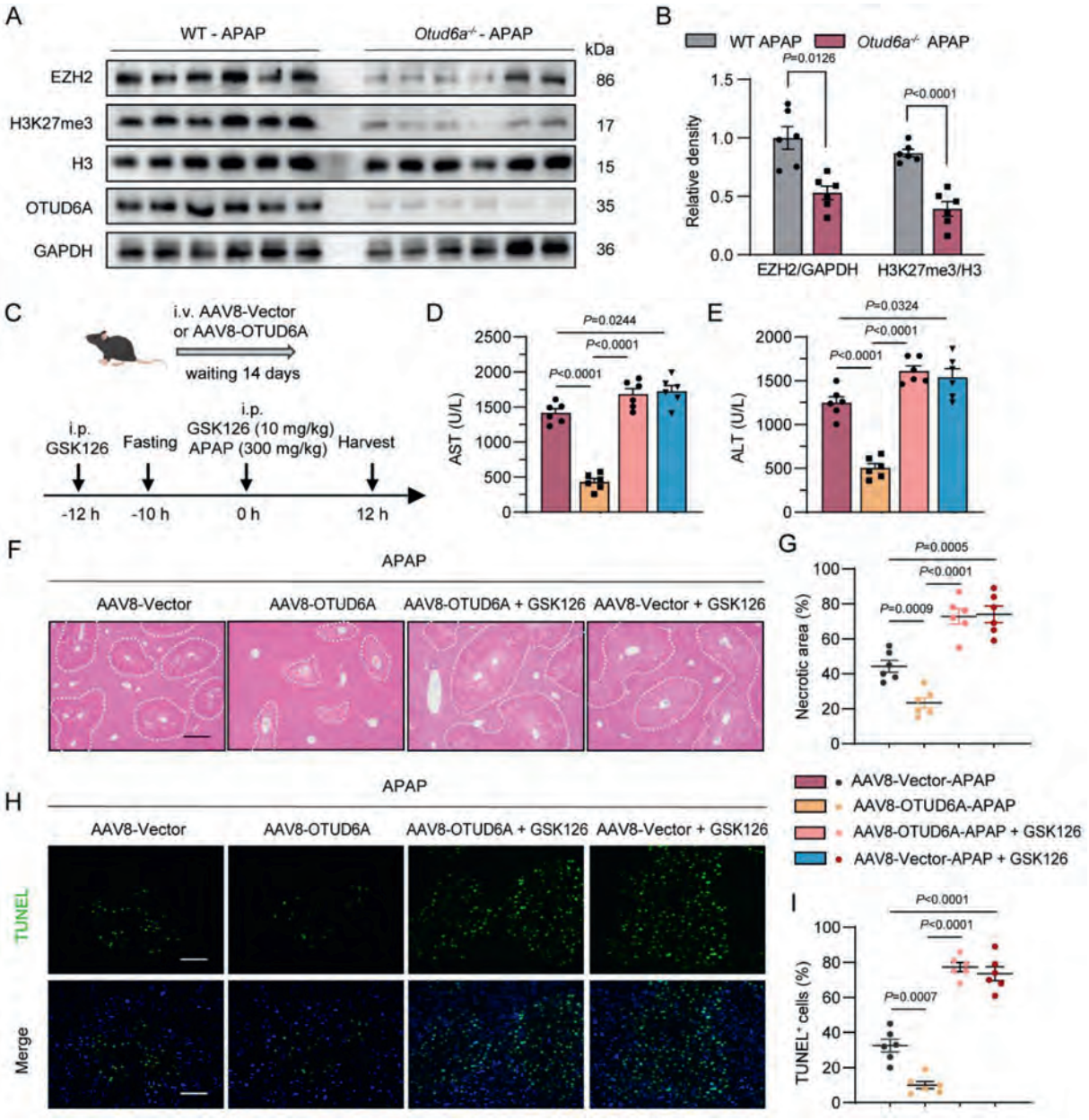

Figure 8 EZH2 mediates the hepatic protection effect of OTUD6A in APAP-treated mice. (A, B) WT and *Otud6a*$^{-/-}$ mice were treated with APAP (250 mg/kg, i.p.) for 12 h. (A) The protein levels of EZH2, H3K27me3, and H3 in the liver tissues were determined using Western blotting assays. Representative immunoblots are shown. GAPDH was used as the loading control. (B) The densitometric quantification data for (A) are shown. (C) Schematic strategy for the experimental timeline of the GSK126 pretreatment in an APAP-induced liver injury mouse model. (D, E) Serum levels of ALT and AST were assayed using commercial kits ($n = 6$). (F, G) Representative images of H&E-stained liver sections (scale bar = 100 μm) and the quantified necrotic areas ($n = 6$) are shown. (H, I) Representative images of TUNEL-stained liver sections (scale bar = 50 μm) and the quantification for the TUNEL-staining are shown ($n = 6$). Statistical data are presented as mean ± SEM.

processes. They are particularly involved in removing ubiquitin chains from target proteins[34]. Targeting certain DUBs, leading to degradation or loss of function of the key proteins, seems to provide a potential therapy for liver diseases. Previous studies have revealed that deregulation or dysfunction of DUBs is always associated with liver diseases. For example, deficiency of A20, a DUB in the OUT family, in liver parenchymal cells spontaneously develops chronic liver inflammation, hepatocyte apoptosis, and lethality following treatment with sublethal doses of TNF[35]. Koschel et al. showed OTUB1 prevents *Listeria monocytogenes* (Lm) and TNF-driven necroptosis of hepatocytes both *in vivo* and *in vitro* and rescued mice from Lm- and D-Gal/TNF-induced mortality[36]. OTUD4 has the ability to inhibit the activation of NF-κB by downregulating K63-linked ubiquitination of TRAF6, which in turn helps mitigate liver ischemia−reperfusion injury[37]. In other reports, OTUD6A promotes prostatic tumorigenesis *via* deubiquitinating and stabilizing different substrate proteins, such as c-Myc, Brg1, and AR[20,38]. OTUD6A has been shown to play important roles in cancer development. For example, OTUD6A is a positive regulator of CDC6, which plays an important role in cell

cycle and chemosensitivity regulation[39]. Recently, our group found that OTUD6A is significantly upregulated in the colons of both DSS-treated mice and ulcerative colitis (UC) patients[40]. OTUD6A stabilizes and activates NLRP3 inflammasome and induces colonic inflammation in macrophages[40]. Here, we found a novel function of OTUD6A in acute inflammatory disease. Our data show increased expression of OTUD6A in both livers and primary hepatocytes after APAP administration. Moreover, OTUD6A deficiency exacerbated APAP-induced liver injury and necrosis, while mice overexpressing OTUD6A alleviated the response to APAP exposure, suggesting OTUD6A as a therapeutic target for treating AILI.

The direct regulation of EZH2 by the ubiquitin system plays an important role in many diseases. Zhang et al. report that ZRANB1 binds, deubiquitinates, and stabilizes EZH2, thus reducing the occurrence of type I diabetes[41]. Guo et al.[42] report that FBW7 destabilizes and accelerates ubiquitin-dependent degradation of EZH2, leading to increased expression of ZBTB16 and reducing the occurrence of type 1 diabetes. More importantly, EZH2 has been identified as essential in liver injury. EZH2 hypermethylates CFTR promoter H3K27me3 and enhances the level of autophagy in homocysteine (Hcy)-treated hepatocytes[43]. In addition, HBx potentiated D-GalN-induced hepatotoxicity and ferroptosis *in vitro via* suppressing SLC7A11 expression through H3K27me3 modification by EZH2[44]. In the present study, we identified EZH2 as a substrate of OTUD6A using liquid chromatography with mass spectrometry/mass spectrometry analysis and verified it by the Co-IP experiments. Moreover, we confirmed that OTUD6A mainly removed K48-linked ubiquitination of EZH2 at K569 and inhibited the proteasomal degradation of EZH2. Future structural biology investigations are needed to further clarify the specific binding site and deubiquitinating mode between OTUD6A and EZH2. To our knowledge, this is the first time to reveal that OTUD6A regulates EZH2 ubiquitination.

In hepatocytes exposed to APAP, ER stress may occur when the accumulation of unfolded or misfolded proteins surpasses the ER's ability to fold them properly. If this stress is too intense or prolonged, it can lead to cellular necrosis[33]. Lysine acetylation and methylation on histones represent significant epigenetic modifications that play a crucial role in controlling the transcription of genes associated with inflammation, oxidative stress, fibrosis, and apoptosis, which arise as a result of maladaptive ER stress[45,46]. Previous research has demonstrated that following the specific knockdown of G9a and EZH2, there is a decrease in the recruitment of these histone methylases, which leads to reduced levels of H3K9me1 and H3K27me3. This reduction correlates with an increase in histone acetylation at the promoter regions of ATF4 and XBP1, ultimately resulting in an upregulation of ATF4 and XBP1 expression. Maintaining methylation of histones H3K9 and H3K27 may help alleviate ER stress, thereby mitigating oxidative stress and the onset of pathological processes that exacerbate renal injury[31]. Here, we identified that OTUD6A mediated APAP-induced primary mouse hepatocytes and liver ER stress and cell death through EZH2. After we inhibited EZH2 with GSK126, the protective effect of OTUD6A on APAP-induced primary hepatocytes was also weakened, suggesting EZH2 is the downstream target of OTUD6A in the AILI mouse model.

It is undeniable that this study has some limitations. A limitation of this study is that we evaluated the function of OTUD6A in liver injury by using whole-body OTUD6A knockout mice rather than the hepatocyte-specific OTUD6A knockout mice. Also, OTUD6A in macrophages has been shown to promote intestinal inflammation and colitis *via* deubiquitination of NLRP3[40]. In this study, we did not further explore whether OTUD6A in macrophages is involved in the pathogenesis of AILI. In the future, hepatocyte OTUD6A-specific knockout mice could be constructed to solve this problem. Another limitation of our study is that, in addition to drug-induced liver injury, acute liver injury has multiple inducible factors. We should use multiple acute liver injury models to confirm the role of OTUD6A in acute liver injury, including the lipopolysaccharide, bile duct ligation, and CCl_4-induced liver injury, to explore the correlation and possible mechanism of OTUD6A.

5. Conclusions

In conclusion, the current study identified upregulated OTUD6A in the liver of APAP-challenged mice and showed that APAP-induced liver injury and necrosis were significantly promoted when OTUD6A was knocked out. Conversely, increased expression of OTUD6A prevented APAP-induced liver injury both *in vivo* and *in vitro*. Mechanistically, we identified EZH2 as an important substrate of OTUD6A. OTUD6A stabilized EZH2 and removed K48-linked ubiquitination of EZH2 at K569, and inhibited the proteasomal degradation of EZH2. To our knowledge, this is the first study to demonstrate that OTUD6A protects APAP-induced liver injury by deubiquitinating EZH2. This finding extends our understanding of the effect of DUBs on APAP-induced liver injury and indicates that OTUD6A is a potential therapeutic target for drug-induced liver injury.

Acknowledgements

We thank Prof. Fuping You (Peking University, Beijing, China) for sharing *Otud6a*$^{-/-}$ mice. This study was supported by the Medical and Health Science Research Project of Zhejiang Province (2022KY348 to Wei Zuo and 2023XY164 to Lijiang Huang, China) and the Key Research Project of Wenzhou City (ZY2021021 to Yi Wang, China).

Author contributions

Yanni Zhao: Writing the original draft, Methodology, Investigation, Data curation. Tianyang Jin: Formal analysis, Data curation, Conceptualization. Tingxin Xu: Investigation. Yi Fang: Investigation. Qingsong Zheng: Investigation. Wu Luo: Investigation. Weiei Zhu: Data curation, Conceptualization. Yue Chen: Conceptualization. Jiong Wang: Visualization, Supervision, Resources. Yi Chen: Project administration, Formal analysis. Wei Zuo: Conceptualization, Funding acquisition. Lijiang Huang: Methodology, Investigation. Guang Liang: Visualization, Validation, Supervision, Resources, Project administration, Conceptualization. Yi Wang: Visualization, Validation, Supervision, Resources, Project administration, Funding acquisition, Conceptualization.

Conflicts of interest

The authors declare no competing interests.

Appendix A. Supporting information

Supporting information to this article can be found online at https://doi.org/10.1016/j.apsb.2025.06.027.

References

1. Kaplowitz N. Idiosyncratic drug hepatotoxicity. *Nat Rev Drug Discov* 2005;**4**:489−99.
2. Steiner RE, Bydder GM. Nuclear magnetic resonance in gastroenterology. *Clin Gastroenterol* 1984;**13**:265−79.
3. Katarey D, Verma S. Drug-induced liver injury. *Clin Med* 2016;**16**: s104−9.
4. Bessot M, Boissel P, Keil L, Boileau F, Hanna F. Vascular anastomoses without suture: applications to hepatic transplantations. *J Chir* 1969; **97**:373−8.
5. Lewis I. Defects in parietal lobe associational patterns in a hypertensive patient. *Ala J Med Sci* 1967;**4**:428−35.
6. Devarbhavi H, Asrani SK, Arab JP, Nartey YA, Pose E, Kamath PS. Global burden of liver disease: 2023 update. *J Hepatol* 2023;**79**: 516−37.
7. Kerr F, Dawson A, Whyte IM, Buckley N, Murray L, Graudins A, et al. The Australasian Clinical Toxicology Investigators Collaboration randomized trial of different loading infusion rates of *N*-acetylcysteine. *Ann Emerg Med* 2005;**45**:402−8.
8. Waring WS, Stephen AF, Robinson OD, Dow MA, Pettie JM. Lower incidence of anaphylactoid reactions to *N*-acetylcysteine in patients with high acetaminophen concentrations after overdose. *Clin Toxicol* 2008;**46**:496−500.
9. Shaid S, Brandts CH, Serve H, Dikic I. Ubiquitination and selective autophagy. *Cell Death Differ* 2013;**20**:21−30.
10. Popovic D, Vucic D, Dikic I. Ubiquitination in disease pathogenesis and treatment. *Nat Med* 2014;**20**:1242−53.
11. Han S, Wang R, Zhang Y, Li X, Gan Y, Gao F, et al. The role of ubiquitination and deubiquitination in tumor invasion and metastasis. *Int J Biol Sci* 2022;**18**:2292−303.
12. Zhu Y, Lei L, Wang X, Chen L, Li W, Li J, et al. The E3 ubiquitin ligase NEDD4-1 protects against acetaminophen-induced liver injury by targeting VDAC1 for degradation. *Acta Pharm Sin B* 2023;**13**: 1616−30.
13. Clague MJ, Coulson JM, Urbe S. Cellular functions of the DUBs. *J Cell Sci* 2012;**125**:277−86.
14. Mevissen TE, Hospenthal MK, Geurink PP, Elliott PR, Akutsu M, Arnaudo N, et al. OTU deubiquitinases reveal mechanisms of linkage specificity and enable ubiquitin chain restriction analysis. *Cell* 2013; **154**:169−84.
15. Lin F, Chen W, Zhou J, Zhu J, Yao Q, Feng B, et al. Mesenchymal stem cells protect against ferroptosis *via* exosome-mediated stabilization of SLC7A11 in acute liver injury. *Cell Death Dis* 2022;**13**: 271.
16. Oikawa D, Gi M, Kosako H, Shimizu K, Takahashi H, Shiota M, et al. OTUD1 deubiquitinase regulates NF-kappaB- and KEAP1-mediated inflammatory responses and reactive oxygen species-associated cell death pathways. *Cell Death Dis* 2022;**13**:694.
17. Zhao Y, Mudge MC, Soll JM, Rodrigues RB, Byrum AK, Schwarzkopf EA, et al. OTUD4 is a phospho-activated K63 deubiquitinase that regulates MyD88-dependent signaling. *Mol Cell* 2018;**69**. 505-16.e5.
18. Qian W, Li Q, Wu X, Li W, Li Q, Zhang J, et al. Deubiquitinase USP29 promotes gastric cancer cell migration by cooperating with phosphatase SCP1 to stabilize Snail protein. *Oncogene* 2020;**39**:6802−15.
19. Shi L, Liu J, Peng Y, Zhang J, Dai X, Zhang S, et al. Deubiquitinase OTUD6A promotes proliferation of cancer cells *via* regulating Drp1 stability and mitochondrial fission. *Mol Oncol* 2020;**14**:3169−83.
20. Peng Y, Liu J, Wang Z, Cui C, Zhang T, Zhang S, et al. Prostate-specific oncogene OTUD6A promotes prostatic tumorigenesis *via* deubiquitinating and stabilizing c-Myc. *Cell Death Differ* 2022;**29**:1730−43.
21. Li Z, Li G, Li Y, Luo Y, Jiang Y, Zhang Z, et al. Deubiquitinase OTUD6A regulates innate immune response *via* targeting UBC13. *Viruses* 2023;**15**:1761.
22. Zhao YN, Liu ZD, Yan T, Xu TX, Jin TY, Jiang YS, et al. Macrophage-specific FGFR1 deletion alleviates high-fat-diet-induced liver inflammation by inhibiting the MAPKs/TNF pathways. *Acta Pharmacol Sin* 2024;**45**:988−1001.
23. Yan M, Huo Y, Yin S, Hu H. Mechanisms of acetaminophen-induced liver injury and its implications for therapeutic interventions. *Redox Biol* 2018;**17**:274−83.
24. Lee WM. Acetaminophen (APAP) hepatotoxicity—isn't it time for APAP to go away?. *J Hepatol* 2017;**67**:1324−31.
25. Liu R, Li Y, Zheng Q, Ding M, Zhou H, Li X. Epigenetic modification in liver fibrosis: promising therapeutic direction with significant challenges ahead. *Acta Pharm Sin B* 2024;**14**: 1009−29.
26. Margueron R, Reinberg D. The polycomb complex PRC2 and its mark in life. *Nature* 2011;**469**:343−9.
27. Chen L, Kang X, Meng X, Huang L, Du Y, Zeng Y, et al. MALAT1-mediated EZH2 recruitment to the GFER promoter region curbs normal hepatocyte proliferation in acute liver injury. *J Clin Transl Hepatol* 2023;**11**:97−109.
28. Jiao K, Yang K, Wang J, Ni Y, Hu C, Liu J, et al. 27-Hydroxycholesterol induces liver fibrosis *via* down-regulation of trimethylation of histone H3 at lysine 27 by activating oxidative stress; effect of nutrient interventions. *Free Radic Biol Med* 2024;**210**: 462−77.
29. Duan R, Du W, Guo W. EZH2: a novel target for cancer treatment. *J Hematol Oncol* 2020;**13**:104.
30. Cao R, Wang L, Wang H, Xia L, Erdjument-Bromage H, Tempst P, et al. Role of histone H3 lysine 27 methylation in polycomb-group silencing. *Science* 2002;**298**:1039−43.
31. Diaz-Bulnes P, Saiz ML, Corte-Iglesias V, Rodrigues-Diez RR, Bernardo Florez A, Ruiz Bernet C, et al. Demethylation of H3K9 and H3K27 contributes to the tubular renal damage triggered by endoplasmic reticulum stress. *Antioxidants* 2022;**11**: 1355.
32. Nagy G, Kardon T, Wunderlich L, Szarka A, Kiss A, Schaff Z, et al. Acetaminophen induces ER dependent signaling in mouse liver. *Arch Biochem Biophys* 2007;**459**:273−9.
33. Li L, Wang H, Zhang J, Sha Y, Wu F, Wen S, et al. SPHK1 deficiency protects mice from acetaminophen-induced ER stress and mitochondrial permeability transition. *Cell Death Differ* 2020; **27**:1924−37.
34. Lv XY, Duan T, Li J. The multiple roles of deubiquitinases in liver cancer. *Am J Cancer Res* 2020;**10**:1647−57.
35. Catrysse L, Farhang Ghahremani M, Vereecke L, Youssef SA, Mc Guire C, Sze M, et al. A20 prevents chronic liver inflammation and cancer by protecting hepatocytes from death. *Cell Death Dis* 2016;**7**: e2250.
36. Koschel J, Nishanth G, Just S, Harit K, Kroger A, Deckert M, et al. OTUB1 prevents lethal hepatocyte necroptosis through stabilization of c-IAP1 during murine liver inflammation. *Cell Death Differ* 2021;**28**: 2257−75.
37. Liu H, Fan J, Zhang W, Chen Q, Zhang Y, Wu Z. OTUD4 alleviates hepatic ischemia−reperfusion injury by suppressing the K63-linked ubiquitination of TRAF6. *Biochem Biophys Res Commun* 2020;**523**: 924−30.
38. Fu X, Zhao J, Yu G, Zhang X, Sun J, Li L, et al. OTUD6A promotes prostate tumorigenesis *via* deubiquitinating Brg1 and AR. *Commun Biol* 2022;**5**:182.
39. Cui J, Liu X, Shang Q, Sun S, Chen S, Dong J, et al. Deubiquitination of CDC6 by OTUD6A promotes tumour progression and chemoresistance. *Mol Cancer* 2024;**23**:86.
40. Liu X, Fang Y, Lv X, Hu C, Chen G, Zhang L, et al. Deubiquitinase OTUD6A in macrophages promotes intestinal inflammation and colitis *via* deubiquitination of NLRP3. *Cell Death Differ* 2023;**30**: 1457−71.
41. Zhang P, Xiao Z, Wang S, Zhang M, Wei Y, Hang Q, et al. ZRANB1 is an EZH2 deubiquitinase and a potential therapeutic target in breast cancer. *Cell Rep* 2018;**23**:823−37.
42. Guo Y, Li J, Fan S, Hu Q. Suppressive role of E3 ubiquitin ligase FBW7 in type I diabetes in non-obese diabetic mice through mediation of ubiquitination of EZH2. *Cell Death Discov* 2021;**7**: 361.

43. Yang A, Jiao Y, Yang S, Deng M, Yang X, Mao C, et al. Homocysteine activates autophagy by inhibition of CFTR expression *via* interaction between DNA methylation and H3K27me3 in mouse liver. *Cell Death Dis* 2018;**9**:169.
44. Liu GZ, Xu XW, Tao SH, Gao MJ, Hou ZH. HBx facilitates ferroptosis in acute liver failure *via* EZH2 mediated SLC7A11 suppression. *J Biomed Sci* 2021;**28**:67.
45. Zhou X, Zang X, Guan Y, Tolbert T, Zhao TC, Bayliss G, et al. Targeting enhancer of zeste homolog 2 protects against acute kidney injury. *Cell Death Dis* 2018;**9**:1067.
46. Majumder S, Thieme K, Batchu SN, Alghamdi TA, Bowskill BB, Kabir MG, et al. Shifts in podocyte histone H3K27me3 regulate mouse and human glomerular disease. *J Clin Investig* 2018;**128**: 483−99.